

Oxidation by-products and ecotoxicity assessment during the photodegradation of fenofibric acid in aqueous solution with UV and UV/H₂O₂

Javier Santiago^a, Ana Agüera^b, María del Mar Gómez-Ramos^b, Amadeo R. Fernández Alba^{b,c}, Eloy García-Calvo^{a,c}, Roberto Rosal^{a,c,*}

^a Department of Chemical Engineering, University of Alcalá, E-28771 Alcalá de Henares, Spain

^b Department of Analytical Chemistry, University of Almería, E-04010 Almería, Spain

^c Advanced Study Institute of Madrid, IMDEA-Agua, Parque Científico Tecnológico, E-28805 Alcalá de Henares, Madrid, Spain

ARTICLE INFO

Article history:

Received 29 April 2011

Received in revised form 11 July 2011

Accepted 18 July 2011

Available online 5 August 2011

Keywords:

Fenofibric acid

UV photolysis

UV/H₂O₂

Toxic by-products

Liquid chromatography

Mass spectrometry

ABSTRACT

The degradation of an aqueous solution of fenofibric acid was investigated using ultraviolet (UV) photolysis and UV/H₂O₂ with a low-pressure mercury lamp. We obtained quantum yields at different temperatures and the rate constant for the reaction of fenofibric acid with hydroxyl radicals. The maximum radical exposure per fluence ratio obtained was $1.4 \times 10^{-10} \text{ ML}^{-1} \text{ mW}^{-1}$. Several reaction intermediates were detected by means of exact mass measurements performed by liquid chromatography coupled to quadrupole-time-of-flight mass spectrometry (LC-ESI-QTOF-MS). UV and UV/H₂O₂ pathways involve the decarboxylation of fenofibric acid to 4-chloro-4'-(1-hydroxy-1-methylethyl)benzophenone and other minor products, predominantly chlorinated aromatics. We detected several intermediates from reactions with hydroxyl radicals and some lower molecular weight products from the scission of the carbonyl carbon-to-aromatic-carbon bond. We recorded high toxicity in UV irradiated samples for the growth of *Pseudokirchneriella subcapitata* even after the total depletion of fenofibric acid; this was probably due to the presence of chlorinated aromatics. A degree of toxicity reappeared in highly irradiated UV/H₂O₂ samples, probably because of the formation of ring-opening products. The degree of mineralization was closely related to that of dechlorination and reached values of over 50% after 3–4 min before stabilizing thereafter.

© 2011 Elsevier B.V. All rights reserved.

1. Introduction

Fenofibric acid, 2-[4-(4-chlorobenzoyl)phenoxy]-2-methylpropanoic acid, is the active form of fenofibrate, a drug prescribed to reduce plasma triglycerides. Although its use is not widespread, it has often been encountered in wastewater treatment plants (WWTP). Rosal et al. [1] reported very low removal efficiency for fenofibric acid in a conventional WWTP located in Madrid with an average annual concentration of 79 ng/L. Stumpf et al. [2] obtained concentrations of up to 500 ng/L in the influent of several Brazilian WWTP and calculated a removal efficiency of 45% for conventional activated sludge treatment. Ternes et al. [3] reported the occurrence of 130 ng/L of fenofibric acid in the effluent of a German WWTP. Acero et al. [4] found 180 ng/L in the effluent of a WWTP located in Madrid. Fenofibric acid attracts particular attention due to its high toxicity for several aquatic microorganisms [5]. An additional reason for concern is that fenofibric acid and other

pharmaceuticals are released in increasing quantities in complex mixtures. Recently, Rodea-Palomares et al. [6] and Rosal et al. [7] used the combination index-isobologram method and reported a synergistic behaviour for fenofibric acid in mixtures involving wastewater.

Advanced oxidation processes (AOP) are effective technologies for the removal of organic pollutants in wastewater. UV-based AOP have the advantage of using a fully commercialized technology due to the widespread use of UV systems for disinfection [8]. A drawback of these processes is the formation of oxidation by-products [9]. Over the last few years, it has been shown that the formation of by-products with enhanced toxicity for non-target organisms usually takes place at least under conditions of moderate carbon removal [10,11]. The identification of unknown transformation products is not an easy task. Liquid chromatography–mass spectrometry (LC–MS) combined with a new generation of high sensitivity MS systems provides abundant structural information for the elucidation of chemical structures. The objective of this work was to study the removal of fenofibric acid using UV and UV/H₂O₂ photolysis. We identified oxidation intermediates in order to propose a reaction pathway for the early oxidation stages. We also measured the ecotoxicity of partially oxidized mixtures.

* Corresponding author at: Department of Chemical Engineering, University of Alcalá, E-28771 Alcalá de Henares, Spain. Tel.: +34 918855099; fax: +34 918855088.
E-mail address: roberto.rosal@uah.es (R. Rosal).

2. Materials and methods

2.1. Reagents

Fenofibric acid was produced from fenofibrate (Sigma–Aldrich, +99% purity) as indicated elsewhere [5]. The product's purity was over 97%, as evaluated by high-performance liquid chromatography (HPLC). Pure water was obtained from a Millipore Mili-Q system with a resistivity of at least 18 M Ω cm at 298 K and a Millipore 0.22 μ m Millipak Express filter (Billerica, MA). Hydrogen peroxide, sodium phosphate monobasic dihydrate and sodium hydrogen phosphate, sodium hydroxide and hydrochloric acid were analytical grade reagents used as received. p-Chlorobenzoic acid (pCBA), atrazine and 2,9-dimethyl-1,10-phenanthroline (DMP) were purchased from Sigma–Aldrich (+99% purity).

2.2. Analytical methods

Total organic carbon (TOC) was determined using a Shimadzu TOC-VCSH analyzer. Chlorine was determined using a Dionex DX120 Ion Chromatograph with a conductivity detector and an IonPac AS9-HC 4 mm \times 250 mm analytical column with ASRS-Ultra suppressor. The eluent was 9.0 mM Na₂CO₃ flowing at 1.0 mL/min. The determination of extinction coefficients and colorimetric analyses was performed in a Shimadzu UV-1800 spectrophotometer. The analyses of fenofibric acid, pCBA and atrazine were performed by HPLC using an Agilent 1200 apparatus equipped with a reversed phase Kromasil 5u 100A C18 analytical column. The mobile phase (flow rate 1 mL/min) was a mixture of water containing 4 mL/L of orthophosphoric acid and 50 mL/L of methanol and acetonitrile in a proportion of 40:60 for pCBA separation and 50:50 for atrazine and fenofibric acid. UV detection was carried out at 280 nm and 228 nm for fenofibric acid, and atrazine and pCBA respectively. The volume injected was 50 μ L in all cases. Hydrogen peroxide was measured using the colorimetric methods of Eisenberg [12] and Baga et al. [13].

A liquid chromatography-electrospray ionization-quadrupole-time-of-flight-mass spectrometry (LC-ESI-QTOF-MS) system, in positive and negative mode, was used to identify the transformation products in the samples. Samples collected at different irradiation times during the experiments were directly analyzed in the LC-TOF-MS system, without previous pre-concentration. The analytes were separated using a HPLC system (vacuum degasser, autosampler and a binary pump Agilent Series 1200, Agilent Technologies) equipped with a reversed-phase XDB-C₁₈ analytical column of 4.6 mm \times 50 mm, 1.8 μ m particle size (Agilent Technologies). 0.1% formic acid and 5% MiliQ water in acetonitrile was used as mobile phase A and 0.1% formic acid in water (pH 3.5) as mobile phase B. The elution gradient went from 10% A (3 min) to 100% A in 22 min, and was kept at 100% A for 3 min. The flow rate was 0.5 mL/min and the injection volume 20 μ L. The HPLC system was connected to a quadrupole-time-of-flight mass spectrometer (Agilent 6530 Q-TOF MS, Agilent Technologies, Santa Clara, CA). The instrument was operated in the 4GHz High Resolution Mode. Ions were generated using an electrospray ion source with Agilent Jet Stream Technology. The operation conditions were: superheated nitrogen sheath gas temperature (400 °C) at flow rate (12 L/min), nozzle voltage (0 V), capillary, 4000 V; nebulizer, 60 psi; drying gas, 5 L/min; gas temperature, 250 °C; skimmer voltage, 65 V; octapoleRFPeak, 750 V; fragmentor (in source CID fragmentation), 90 V. The mass axis was calibrated using the mixture provided by the manufacturer over the m/z 40–3200 range. A second sprayer with a reference solution was used for continuous calibration in positive ion using the following reference masses: 121.0509 and 922.0098 m/z (resolution: 21,700 \pm 500 at 922.0098 m/z), and in negative ion using the reference masses: 112.9856 and 966.0007.

MS/MS spectra were acquired over the m/z 40–950 range at a scan rate of 0.5 s/spectrum. The collision energy was optimized to obtain the highest number of fragments. The full mass spectra data recorded were processed with Agilent MassHunter Workstation Software (version B.02.00).

2.3. Toxicity test and data analysis

The toxicities of fenofibric acid degradations by UV and UV/H₂O₂ treatments were evaluated in accordance with the algal growth inhibition test described in OECD TG 201 and using the *Pseudokirchneriella subcapitata* open system. Prior to the test, hydrogen peroxide was removed using 4 μ L of catalase solution 5000 mg/L (3691 U/mg bovine liver from Sigma–Aldrich) per 1 mL of sample. Cultures were made in OECD growth medium at pH 8.0 \pm 0.2. Algal cells were first cultured in 25 mL agitated flasks, in which growth was evaluated by cell counting. The prescribed amount of cells were then transferred to 96-well clear disposable microplates and exposed to pollutants during the logarithmic growth phase. The total volume occupied was 200 μ L, each well containing 100 μ L of sample and 100 μ L of OECD growth medium. The microplates were placed in an algal growth chamber under continuous fluorescent illumination (approximately 100 μ E m² s⁻¹), and incubated at 22 \pm 1 °C. The cell density was measured using an electronic particle counter (Coulter Counter Z2). The settings were: upper size limit, 8.0 μ m; lower size limit, 2.5 μ m; metered volume, 0.5 mL; aperture size, 50 μ m. The tests were carried out with duplicate samples for each day of measurement and samples were taken at 24-h intervals over 72 h. Specific growth rates were calculated for each sample and treatment in order to obtain the inhibition percentage. EC₅₀ value and 95% confidence limits for fenofibric acid were calculated using the concentration–inhibition relationship established by the logistic equation.

2.4. Experimental setup and procedure

Irradiation experiments were performed in a Heraeus 700 mL reactor equipped with a 15 W Heraeus Noblelight TNN 15/32 low-pressure mercury vapour lamp emitting at 254 nm with a secondary peak at 185 nm. The inner and outer radiuses were 2.4 and 4.5 cm respectively and the height of irradiated solution was 17 cm. The reactor was covered with black paper to avoid any reflection and in order to maintain a constant temperature the lamp was fitted in a quartz cooling tube refrigerated by means of a Huber Polystat cc2 thermostatic regulator. pH was kept constant using a 4 mM phosphate buffer; pH was monitored periodically to ensure a constant value within \pm 0.1 units. The experiments were carried out in batch mode and samples were withdrawn for analysis at set intervals.

Hydrogen peroxide actinometry experiments were performed to determine fluence rate. With respect to the annular geometry of the photoreactor, we assumed a linear source with emission in planes parallel to the lamp axis (LSPP). In this model the lamp is viewed as a consecutive line of points, each emitting radiation radially in all directions. The equation for the fluence rate is:

$$E'(r) = \frac{E'_0 R_0}{r} e^{-\mu(r-R_0)} \quad (1)$$

where μ is the attenuation coefficient, R_0 the radius of the internal wall of the photoreactor and E'_0 the fluence rate at R_0 expressed in mW cm⁻². By applying the LSPP model to the UV photolysis of hydrogen peroxide at high concentration, the exponent becomes negligible and the rate of hydrogen peroxide photolysis allows the

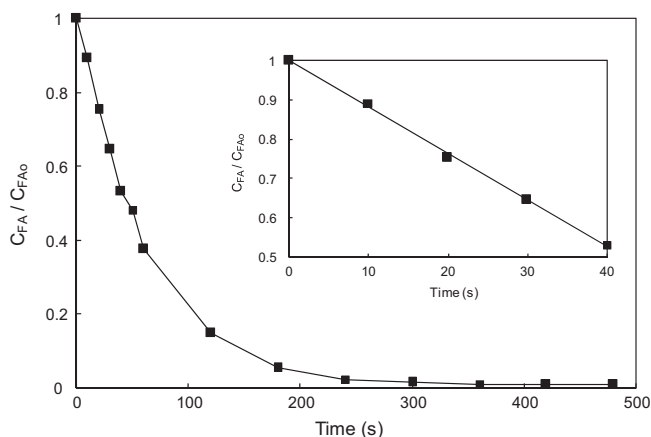


Fig. 1. Photolytic decomposition of fenofibric acid at 35 °C and pH 6.5. The inset represents the period for which the reaction followed zero order kinetics.

fluence rate to be determined at the internal wall of the photoreactor, E'_0 :

$$-\frac{dc_{H_2O_2}}{dt} = \Phi_{H_2O_2} \frac{2\pi R_0 L E'_0}{V} \quad (2)$$

The total hydrogen peroxide quantum yield, $\Phi_{H_2O_2}$, was considered to be 1 mol E^{-1} at 254 nm [14]. Using 0.05 M of H_2O_2 , we determined that the fluence rate was $18.73 \pm 0.23 \text{ mW cm}^{-2}$. For a low attenuation coefficient, the photolytic decomposition of hydrogen peroxide follows a first order rate equation where $\varepsilon_{H_2O_2}$ is the molar extinction coefficient of hydrogen peroxide at 254 nm:

$$-\frac{dc_{H_2O_2}}{dt} = 2.303 \frac{2\pi R_0 L E'_0 \varepsilon_{H_2O_2}}{V} (R_1 - R_0) c_{H_2O_2} \quad (3)$$

From experiments at 10^{-4} M of H_2O_2 , we obtained an effective path of radiation through the reactor of $2.37 \pm 0.07 \text{ cm}$, essentially coincident with the physical value of $R_1 - R_0$. More details concerning equations and experimental procedure can be found elsewhere [15].

3. Results and discussion

3.1. UV photolysis

The molar extinction coefficient of fenofibric acid at pH 6.5 and 254 nm was $9199 \pm 150 \text{ M}^{-1} \text{ cm}^{-1}$, a value that we did not find elsewhere. As for hydrogen peroxide, atrazine and pCBA, we measured 19.3 ± 0.3 , 3768 ± 55 and $2760 \pm 94 \text{ M}^{-1} \text{ cm}^{-1}$ respectively in agreement with previously reported extinction coefficients [8,16,17]. The photolysis rate of a single target compound at an arbitrary concentration level is given by:

$$-\frac{dc_A}{dt} = \Phi_A \frac{2\pi R_0 L E'_0}{V} [1 - e^{-\mu(R_1 - R_0)}] \quad (4)$$

At high concentrations of the absorbing compound, the integration of the former equation yields the following zero order kinetics:

$$c_A(t) = c_{A_0} - \Phi_A \frac{2\pi R_0 L E'_0}{V} t \quad (5)$$

Fig. 1 shows the data corresponding to a photolytic decomposition of fenofibric acid. The inset represents a plot of Eq. (5) during the period in which $2.303\varepsilon_A c_A (R_1 - R_0) > 2$, which is its conventional validity condition. We obtained quantum yields for fenofibric acid at 15 °C ($0.039 \pm 0.003 \text{ mol E}^{-1}$), 25 °C ($0.065 \pm 0.003 \text{ mol E}^{-1}$) and 35 °C ($0.088 \pm 0.002 \text{ mol E}^{-1}$). These data correspond to an activation energy for the photolysis rate of $21.5 \pm 8.6 \text{ kJ mol}^{-1}$. The same values for the photolysis of atrazine were $0.040 \pm 0.003 \text{ mol E}^{-1}$

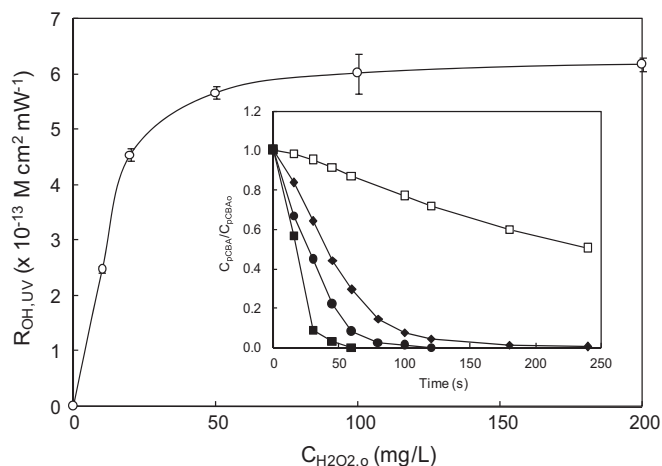


Fig. 2. $R_{OH,UV}$ for different initial concentrations of hydrogen peroxide and (inset) evolution of the concentration of pCBA for runs without H_2O_2 (\square) and using 10 mg/L H_2O_2 (\blacklozenge), 50 mg/L H_2O_2 (\blacktriangle) and 100 mg/L H_2O_2 (\blacksquare).

at 15 °C, $0.053 \pm 0.002 \text{ mol E}^{-1}$ at 25 °C and $0.055 \pm 0.001 \text{ mol E}^{-1}$ at 35 °C with an activation energy of $11.9 \pm 4.7 \text{ kJ mol}^{-1}$. The values found for atrazine were in good agreement with previously reported data [18]. However, the only value found for the quantum yield of fenofibric acid, reported by Miranda et al. [19], is considerably higher, $\sim 0.6 \text{ mol E}^{-1}$, a discrepancy that may be attributed to the different wavelength used (355 nm).

3.2. Kinetics of UV/ H_2O_2 process

The radical exposure per fluence ratio due to the irradiation, $R_{OH,UV}$, and the stationary-state concentration of HO^\bullet radicals was determined according to the method proposed by Rosenfeldt and Linden [20]:

$$R_{OH,UV} = \frac{\int_0^t C_{HO^\bullet} dt}{E'_0 t} \quad (6)$$

Following Rosenfeldt et al. [21], we used pCBA as the radical probe compound for determining HO^\bullet exposure. The rate of depletion of pCBA by the UV/ H_2O_2 process is given by the following equation in which F_{pCBA} is the fraction of total radiation absorbed by pCBA:

$$-\frac{dc_{pCBA}}{dt} = (F_{pCBA} k_{d,pCBA} + k_{HO^\bullet,pCBA} c_{HO^\bullet}) c_{pCBA} \quad (7)$$

Integrating Eq. (7) gives the following expression:

$$\ln \frac{c_{pCBA,o}}{c_{pCBA}} = F_{pCBA} k_{d,pCBA} t + \int c_{HO^\bullet} dt \quad (8)$$

The combination of Eqs. (6)–(8) allowed $R_{OH,UV}$ to be calculated under different reaction conditions. The results, shown in Fig. 2, indicated that $R_{OH,UV}$ was strongly dependent on the presence of hydrogen peroxide, with values of up to $6 \times 10^{-13} \text{ M cm}^2 \text{ mW}^{-1}$ at a plateau reached at about 50 mg/L H_2O_2 . These values bear comparison with those for HO^\bullet radical availability obtained by Rosenfeldt et al. [21] during the irradiation of water from several Swiss lakes; that is to say, volume-based $R_{OH,UV}$ in the $1\text{--}4 \times 10^{-13} \text{ ML}^{-1} \text{ mW}^{-1}$ range for 10 mg/L H_2O_2 under low-pressure mercury vapour irradiation. In our work, we measured $5.7 \times 10^{-11} \text{ ML}^{-1} \text{ mW}^{-1}$ which dropped to $1.8 \times 10^{-11} \text{ ML}^{-1} \text{ mW}^{-1}$ in the presence of 10 mg/L of fenofibric acid. This difference reflects the presence of radical scavengers and UV absorbers in natural water. The inset in Fig. 2 shows the oxidation profiles of pCBA without H_2O_2 and in the presence of 10, 50 and 100 mg/L H_2O_2 . Above 200 mg/L, the radical exposure per fluence ratio starts to decline as a consequence of the well-

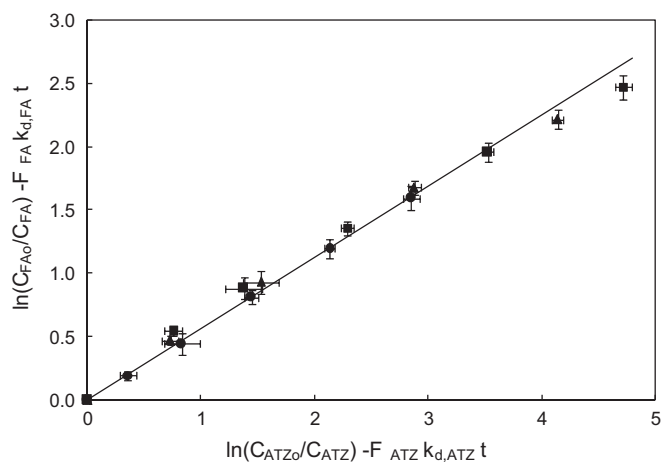


Fig. 3. Plot of the competitive method of kinetic analysis during UV/H₂O₂ oxidation of mixtures of FA and ATZ using 50 mg/L H₂O₂ (●), 100 mg/L H₂O₂ (■) and 200 mg/L H₂O₂ (▲). (95% confidence intervals are shown for reference.)

known effect of overdosing hydrogen peroxide, which reacts with HO• to form hydroperoxyl radicals.

The photolysis rate given by Eq. (3) also holds when two or more compounds are simultaneously photodegraded [17]. In this case, the rate expressions for a given couple of solutes can be written in the form of competitive kinetics:

$$\ln \frac{C_{A,0}}{C_A(t)} - F_A k_{d,A} t = \frac{k_{HO^{\bullet},A}}{k_{HO^{\bullet},B}} \left[\ln \frac{C_{B,0}}{C_B(t)} - F_B k_{d,B} t \right] \quad (9)$$

The data plotted in Fig. 3 correspond to the irradiation of a mixture of fenofibric acid and atrazine using 50, 100 and 200 mg/L H₂O₂. The reason for using atrazine instead of pCBA is that the latter is also a product of the photodegradation of fenofibric acid, as indicated below. The slope of the plot shown in Fig. 3 allowed the second order rate constant for the reaction of fenofibric acid with hydroxyl radicals to be determined. To do so, we used the value of Balci et al. [22] for the rate constant of atrazine with hydroxyl radicals, which is the only value available that indicates uncertainty. The rate constant for the oxidation of fenofibric acid with HO• was $(5.56 \pm 0.22) \times 10^9 \text{ M}^{-1} \text{ s}^{-1}$, a value close to that obtained before in ozonation runs [23]. By performing runs at different pH in the 5.5–7.5 interval, we could also determine that the rate constant for the oxidation of fenofibric acid did not depend on pH, with deviations from the mean not exceeding 5%, while there was almost complete overlapping of confidence intervals. In UV/H₂O₂ runs performed at free pH in the absence of any buffer we noted a continuous trend towards acidification, while in UV photolytic experiments pH increased slightly during the first 2–4 min of irradiation before decreasing thereafter. This behaviour was attributed to the formation of acidic compounds due to the oxidation of intermediates by hydroxyl radicals or other oxidizing species formed during the process.

3.3. Identification of reaction intermediates and reaction pathway

Although UV and UV/H₂O₂ can lead to the total removal of fenofibric acid in a few minutes under the experimental conditions tested in this work, this was never accompanied by complete mineralization. The maximum TOC removal observed for UV/H₂O₂ was slightly over 50% after 4 min of UV/H₂O₂ oxidation, but most of the organic carbon removed disappeared during the first minute (Fig. 4). The analysis of chloride in solution gave concordant results, with a degree of dechlorination of about 60% after 3 min that increased only up to 66% after 15 min when 20 mg/L of fenofib-

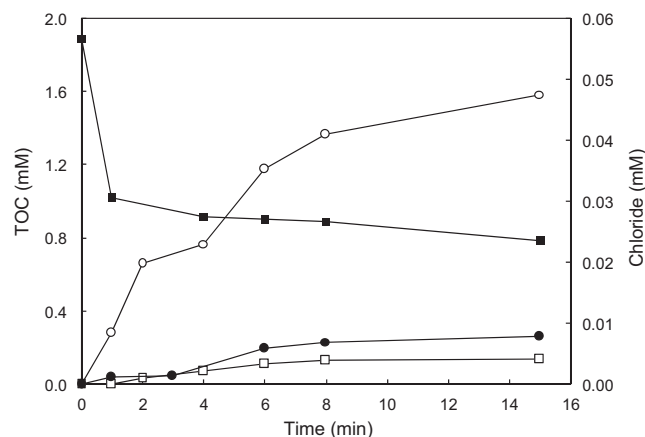


Fig. 4. Evolution of TOC during UV/H₂O₂ using 50 mg/L H₂O₂ (■, left) and organic carbon in acetate, formate and oxalate during the same run (●, left). Increase of chloride in solution during UV/H₂O₂ (50 mg/L, ○, right) and UV (□, right).

ric acid were irradiated in the presence of 50 mg/L of H₂O₂ (pH 6.5, 25 °C). UV irradiation led to a degree of dechlorination typically below 10% and accompanied by very limited TOC removal. Therefore, certain degradation by-products refractory to dechlorination and oxidation persisted after the total removal of the parent compound. This fact highlights the need to characterize reaction mixtures in order to identify persistent and toxic compounds.

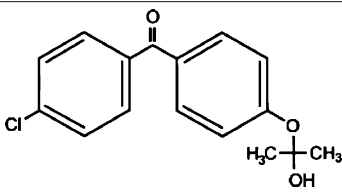
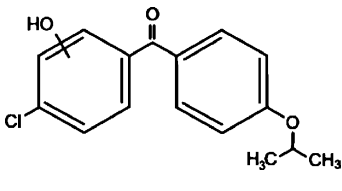
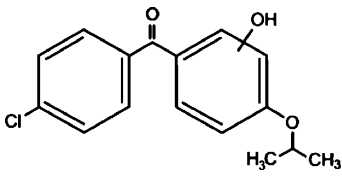
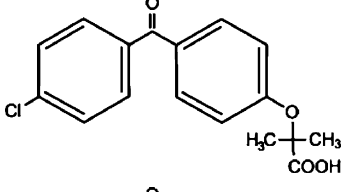
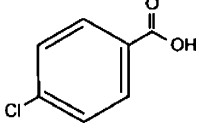
The identification of fenofibric acid photolysis and oxidation by-products was based on the accurate mass measurements recorded by the LC-ESI-QTOF-MS instrument described above, operating in positive (ESI+) and negative modes (ESI-). These measurements allowed elemental compositions to be proposed for both protonated [M-H]⁺ or deprotonated [M-H]⁻ molecular ions and characteristic ion fragments obtained by in-source fragmentation, which provide a high degree of confidence in structure assignment. Fig. 5 shows LC-ESI-QTOF-MS/MS spectra of UV/H₂O₂ and UV transformation products of fenofibric acid, while Tables 1 and 2 list the ion formula and calculated mass of the ions, as well as relative mass error and DBE (double bond and ring equivalents). Table 1 refers to the products of UV photolysis of fenofibric acid, whereas Table 2 gives the compounds identified during UV/H₂O₂ treatments. The accurate mass measurements recorded for the protonated and deprotonated fenofibric acid molecule (*m/z* 319.0732 for C₁₇H₁₆ClO₄ and 317.0586 for C₁₇H₁₄ClO₄) yielded excellent agreement between experimental and calculated *m/z* values, with less than 1.7 ppm error. The observation of the characteristic fragmentation of the parent drug provided information for the identification of transformation products. The appearance of fragments characteristic of the parent molecule in the product spectra indicates the prevalence of a certain fraction of the molecule, suggesting that the transformation takes place in another part of the structure.

The proposed reaction pathway for UV photolysis is shown in Fig. 6a. The primary photoproducts identified in this work were the isomers P-275a and P-275b (C₁₆H₁₆ClO₂, *m/z* 275.0833) and compound P-233 (C₁₃H₁₀ClO₂, *m/z* 233.0364). P-275a (4-chloro-4'-(1-hydroxy-1-methylethyl)benzophenone) and P-275b (4-chloro-4'-isopropoxybenzophenone) correspond to the decarboxylation of fenofibric acid. The photodegradation of fenofibric acid has been attributed to the presence of the easily photo-excited benzophenone group. The first reaction would be a decarboxylation involving a radical species formed via a photo-ionization process upon electron release followed by loss of carbon dioxide [24]. P-233 (4-chloro-4'-hydroxybenzophenone) is the result of the cleavage of the ether with loss of 2-methylpropanoate. As indicated in Fig. 7,

Table 1
Accurate mass measurements of fenofibric acid and its UV photolysis products by LC-ESI-QTOF-MS and structures proposed for the identified transformation products.

Compound	R_t (min)	Ion mass (m/z)	Ion formula	Error (ppm)	DBE	Proposed structure
<i>(a) ESI(+)</i>						
Fenofibric acid (FA)	18.76	319.0732	$C_{17}H_{16}ClO_4$	-1.80	10	
		233.0364	$C_{13}H_{10}ClO_2$	1.01	8.5	
		138.9945	C_7H_4ClO	0.80	5.5	
		121.0284	$C_7H_5O_2$	4.34	5.5	
P-233	17.08	233.0364	$C_{13}H_{10}ClO_2$	0.90	9	
		138.9945	C_7H_4ClO	1.46	4	
		121.0284	$C_7H_5O_2$	0.02	5.5	
		110.9996	C_6H_4Cl	3.75	4.5	
P-249a	14.40	249.0313	$C_{13}H_{10}ClO_3$	-1.30	9	
		125.9843	C_6H_3ClO	4.60	5	
		121.0284	$C_7H_5O_2$	9.07	5.5	
P-249b	15.43	249.0313	$C_{13}H_{10}ClO_3$	-1.89	9	
		147.0441	$C_9H_7O_2$	-1.62	6.5	
		138.9945	C_7H_4ClO	-1.97	5.5	
P-257a	13.06	257.1172	$C_{16}H_{17}O_3$	-1.49	9	
		215.0703	$C_{13}H_{11}O_3$	4.20	8.5	
		121.0284	$C_7H_5O_2$	-2.15	5.5	
P-257b	17.40	257.1172	$C_{16}H_{17}O_3$	-3.70	9	
		215.0703	$C_{13}H_{11}O_3$	3.74	8.5	
		121.0284	$C_7H_5O_2$	-3.62	5.5	
P-275a	18.30	275.0833	$C_{16}H_{16}ClO_2$	-2.11	9	
		257.0728	$C_{16}H_{14}ClO$	-2.01	9.5	
		217.0415	$C_{13}H_{10}ClO$	-2.39	8.5	
		163.0754	$C_{10}H_{11}O_2$	-3.10	5.5	
		138.9945	C_7H_4ClO	-4.09	5.5	
		119.0855	C_9H_{11}	-4.83	4.5	
		105.0335	C_7H_5O	-5.14	5.5	
		73.0284	$C_3H_5O_2$	-7.60	1.5	
59.0491	C_3H_7O	-9.89	0.5			
P-275b	23.24	275.0833	$C_{16}H_{16}ClO_2$	-3.99	9	
		233.0364	$C_{13}H_{10}ClO_2$	2.02	8.5	
		138.9945	C_7H_4ClO	1.22	5.5	
		121.0284	$C_7H_5O_2$	-1.12	5.5	
		110.9996	C_6H_4Cl	-1.06	4.5	

Table 1 (Continued)

Compound	R _t (min)	Ion mass (m/z)	Ion formula	Error (ppm)	DBE	Proposed structure
P-291a	17.72	291.0782	C ₁₆ H ₁₆ ClO ₃	−4.66	9	
		233.0364	C ₁₃ H ₁₀ ClO ₂	2.45	8.5	
		138.9945	C ₇ H ₄ ClO	−3.99	5.5	
		121.0284	C ₇ H ₅ O ₂	−9.60	5.5	
P-291b	19.74	291.0782	C ₁₆ H ₁₆ ClO ₃	−4.66	9	
		249.0313	C ₁₃ H ₁₀ ClO ₃	2.45	8.5	
		154.9894	C ₇ H ₄ ClO ₂	−3.99	5.5	
		121.0284	C ₇ H ₅ O ₂	−9.60	5.5	
P-291c	20.03	291.0782	C ₁₆ H ₁₆ ClO ₃	−0.56	9	
		249.0313	C ₁₃ H ₁₀ ClO ₃	4.53	8.5	
		138.9945	C ₇ H ₄ ClO	−3.91	5.5	
(b) ESI(−)						
Fenofibric acid (FA)	18.78	317.0586	C ₁₇ H ₁₄ ClO ₄	−1.35	10	
		231.0218	C ₁₃ H ₈ ClO ₂	−0.10	9	
pCBA, P-155	13.90	154.9905	C ₇ H ₄ ClO ₂	0.09	5	
		111.0007	C ₆ H ₄ Cl	−3.18	4	

P-275b is the major identified photoproduct in irradiated mixtures, with minor amounts of P-233 and P-291a. These primary photoproducts agree with those found previously by Cosa [25], who reported that the excitation of the carboxylate form of fenofibric acid in aqueous buffer at pH 7.4 generates an excited state that decarboxylates to produce a transient biradical intermediate (BRI in Fig. 6). This intermediate undergoes intersystem crossing and protonation to yield two products, also identified in this work as P-275a and P-275b. Boscá and Miranda [26] used laser flash photolysis at 355 nm to study the photodegradation of fenofibric acid. They found the same photoproducts, with similar concentrations of both isomers (P-275a and P-275b). They also encountered P-233, which was attributed to oxygen trapping by an excited state of fenofibric acid or BRI, the later being the option displayed in Fig. 6a. In agitated runs under air, the concentration of dissolved oxygen was typically in the 7–8 mg/L range at 25 °C. We also detected P-291a, which is probably the consequence of the uptake of oxygen by BRI.

In this work we were also able to detect several reaction products derived from fenofibric acid or its primary products with hydroxyl radicals. The most significant was pCBA (P-155), detected in negative ESI ionization mode (C₇H₄ClO₂, m/z 154.9905), whose ion fragment C₆H₄Cl (m/z 111.0007) revealed a non-substituted aromatic moiety. pCBA could be a product of the reaction of HO• radicals with fenofibric acid and also with photoproducts P-291a, P-291c, P-275a, P-275b or P-233. For the sake of clarity and to stress the fact that we did not find hydroxylated forms of pCBA, we have

only included the first possibility in Fig. 6a. The presence of intermediates giving evidence of the hydroxylation of aromatic rings can be explained by the vacuum ultraviolet (VUV) irradiation of low-pressure mercury lamps at 185 nm (about 5% of the total power for the lamp used in this work). The greater effectiveness of VUV irradiation is a consequence of the formation of hydroxyl radicals via the photolysis of water at 185 nm [27]. It is well-known that 185 nm VUV may also produce ozone from dissolved oxygen. We detected small amounts of dissolved ozone but we did not find any reaction product that could be associated with ozone such as ring-opening by ozone cycloaddition [10].

Fig. 6b shows the proposed pathway for the UV/H₂O₂ oxidation of fenofibric acid. The details concerning the identification and structure proposal are given in Table 2. The intermediates observed during the photolytic experiments were also identified in UV/H₂O₂ samples. These are compounds P-291a, P-275a, P-275b and P-233, coincident with those indicated before, and two additional intermediates derived from fenofibric acid, P-335 (C₁₇H₁₆ClO₅, m/z 335.0681) and P-351 (C₁₇H₁₆ClO₆, m/z 351.0630), the elemental composition of which, containing one and two HO groups more than fenofibric acid and without alteration of DBE, corresponded to hydroxylated derivatives. No exact position for hydroxyl groups can be proposed from the fragmentation pattern (Table 2). A similar couple of hydroxylation derivatives could be attributed to HO• attack on P-233, namely P-249a and P-249b. In this case, the fragmentation allowed the hydroxylated ring to be identified. The

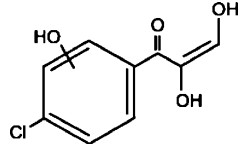
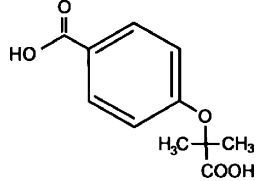
Table 2
Accurate mass measurements of fenofibric acid and its UV/H₂O₂ products by LC-ESI-QTOF-MS and structures proposed for the identified transformation products.

Compound	R _t (min)	Ion mass (m/z)	Ion formula	Error (ppm)	DBE	Proposed structure
<i>(a) ESI(+)</i>						
Fenofibric acid (FA)	18.76	319.0732	C ₁₇ H ₁₆ ClO ₄	-1.65	10	
		233.0364	C ₁₃ H ₁₀ ClO ₂	1.49	8.5	
		138.9945	C ₇ H ₄ ClO	-1.19	5.5	
		121.0284	C ₇ H ₅ O ₂	-9.21	5.5	
P-233	17.15	233.0364	C ₁₃ H ₁₀ ClO ₂	2.75	9	
		138.9945	C ₇ H ₄ ClO	4.00	4	
		121.0284	C ₇ H ₅ O ₂	5.84	5.5	
		110.9996	C ₆ H ₄ Cl	4.72	4.5	
P-249a	14.44	249.0313	C ₁₃ H ₁₀ ClO ₃	-1.20	9	
		125.9843	C ₆ H ₃ ClO	3.20	5	
		121.0284	C ₇ H ₅ O ₂	16.1	5.5	
P-249b	15.43	249.0313	C ₁₃ H ₁₀ ClO ₃	4.43	9	
		147.0441	C ₉ H ₇ O ₂	-14.2	6.5	
		138.9945	C ₇ H ₄ ClO	-1.87	5.5	
		125.9867	C ₆ H ₃ ClO	4.80	5	
P-257	17.44	257.1172	C ₁₆ H ₁₇ O ₃	9.43	9	
		215.0703	C ₆ H ₃ ClO	4.43	8.5	
		121.0284	C ₇ H ₅ O ₂	-4.25	5.5	
P-275a	18.50	275.0833	C ₁₆ H ₁₆ ClO ₂	-2.12	9	
		138.9945	C ₇ H ₄ ClO	-4.09	5.5	
		110.9996	C ₆ H ₄ Cl	-4.98	4.5	
		59.0491	C ₃ H ₇ O	-9.99	0.5	
P-275b	23.32	275.0833	C ₁₆ H ₁₆ ClO ₂	-2.74	9	
		233.0364	C ₁₃ H ₁₀ ClO ₂	2.02	8.5	
		138.9945	C ₇ H ₄ ClO	1.22	5.5	
		121.0284	C ₇ H ₅ O ₂	-1.12	5.5	
		110.9996	C ₆ H ₄ Cl	-1.06	4.5	
P-291a	17.79	291.0782	C ₁₆ H ₁₆ ClO ₃	-1.27	9	
		233.0364	C ₁₃ H ₁₀ ClO ₂	3.62	8.5	
		138.9945	C ₇ H ₄ ClO	-8.12	5.5	
		121.0284	C ₇ H ₅ O ₂	-9.60	5.5	

Table 2 (Continued)

Compound	R_t (min)	Ion mass (m/z)	Ion formula	Error (ppm)	DBE	Proposed structure
P-291b	19.83	291.0782	$C_{16}H_{16}ClO_3$	3.91	9	
		249.0313	$C_{13}H_{10}ClO_3$	4.94	8.5	
		154.9894	$C_7H_4ClO_2$	-3.42	5.5	
		121.0284	$C_7H_5O_2$	1.66	5.5	
P-291c	20.11	291.0782	$C_{16}H_{16}ClO_3$	-0.13	9	
		249.0313	$C_{13}H_{10}ClO_3$	5.72	8.5	
		138.9945	C_7H_4ClO	-6.03	5.5	
		110.9996	C_6H_4Cl	3.05	4.5	
P-307	19.11	307.0732	$C_{16}H_{16}ClO_4$	-2.26	9	
		247.0156	$C_{13}H_8ClO_3$	4.87	9.5	
		184.0519	$C_{12}H_8O_2$	-2.26	9	
P-335	16.24	335.0681	$C_{17}H_{16}ClO_5$	2.26	10	
		249.0313	$C_{13}H_{10}ClO_3$	1.92	8.5	
P-351	16.01	351.0630	$C_{17}H_{16}ClO_6$	1.13	10	
		247.0516	$C_{13}H_8ClO_3$	15.6	9.5	
(b) ESI(-)						
Fenofibric acid (FA)	18.78	317.0586	$C_{17}H_{14}ClO_4$	-1.78	10	
		231.0218	$C_{13}H_8ClO_2$	-0.60	9	
pCBA, P-155	13.90	154.9905	$C_7H_4ClO_2$	0.05	5	
		111.0007	C_6H_4Cl	1.17	4	
P-195	9.96	195.0663	$C_{10}H_{11}O_4$	0.61	5	

Table 2 (Continued)

Compound	R _t (min)	Ion mass (m/z)	Ion formula	Error (ppm)	DBE	Proposed structure
P-213	14.41	212.9960	C ₉ H ₆ ClO ₄	-3.42	6	
		154.9905	C ₇ H ₄ ClO ₂	-2.18	5	
P-223	11.51	223.0612	C ₁₁ H ₁₁ O ₅	-0.12	6	
		137.0244	C ₇ H ₅ O ₃	-1.43	5	

hydroxylation products from P-275b also coincided with those encountered in photolytic runs plus compound P-257 (C₁₆H₁₇O₃, *m/z* 257.1172), the only one identified with the loss of the original chlorine atom. Similar reasoning was applied to the identification of P-307 (C₁₆H₁₆ClO₄, *m/z* 307.0732), a product of HO[•] attack on P-291a. In ESI⁻, we detected four additional intermediates, the most abundant of which was pCBA. In this case, we were able to detect the other fragment from the scission of the carbonyl carbon to aromatic carbon bond, P-195 (C₁₀H₁₁O₄, *m/z* 195.0663) and the symmetric product P-223 (C₁₁H₁₁O₅, *m/z* 223.0612). Another minor product, P-213 (C₉H₆ClO₄, *m/z* 212.9960), was probably the consequence of the hydroxyl attack and ring opening of fenofibric acid, but it could also be a product of any of the chlorine-containing compound with two aromatic rings listed in Table 2.

3.4. Toxicity of partially oxidized mixtures

Fig. 7 shows the growth inhibition of *P. subcapitata* when exposed to fenofibric acid and partially irradiated or oxidized mix-

tures as a function of the duration of treatment. The median effect value for the toxicity of fenofibric acid was 7.90 ± 1.61 mg/L, where the boundaries represent 95% confidence intervals. The value was obtained by fitting dose–response data to a logistic function. The results showed that toxicity decreased slightly during the first minute under UV and UV/H₂O₂, but reached a plateau for UV runs with a maximum at about 6 min. Besides, growth inhibition remained in the 20–40% range after the first minute and throughout the run. UV/H₂O₂ oxidation, on the other hand, allowed toxicity to be eliminated completely at about 4 min. After that, we observed a new increase in toxicity with a relative maximum somewhat in advance of that found in irradiation runs. The bars represent standard deviations for four replicated runs. This behaviour was attributed to a balance between the disappearance of the relatively toxic parent compound and the formation of toxic products. Cosa [25] used molecular a priori analysis based on excited-state lifetimes and singlet oxygen sensitization to predict that the phototoxicity of irradiation products from fenofibric acid should be attributed to P-275a. We found, however, that P-275a was a very

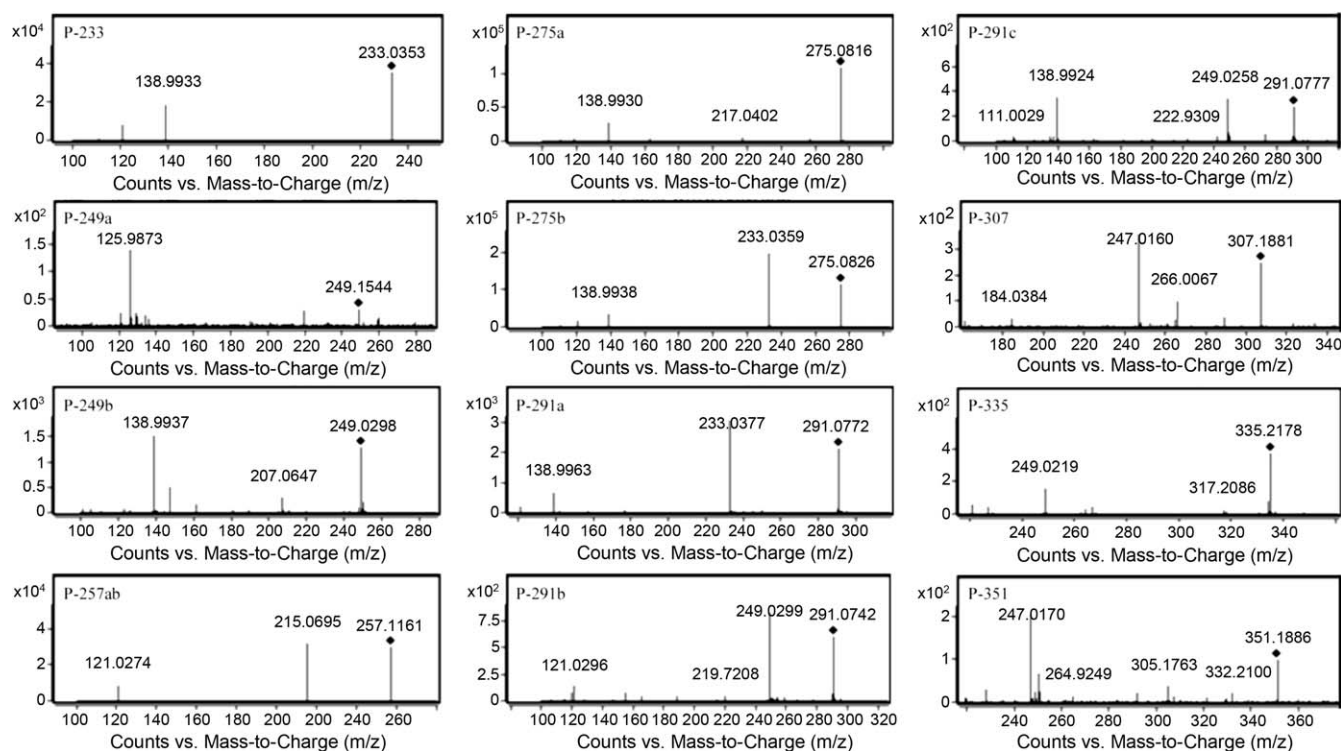


Fig. 5. LC-ESI-QTOF-MS/MS spectra of UV/H₂O₂ and UV transformation products of fenofibric acid.

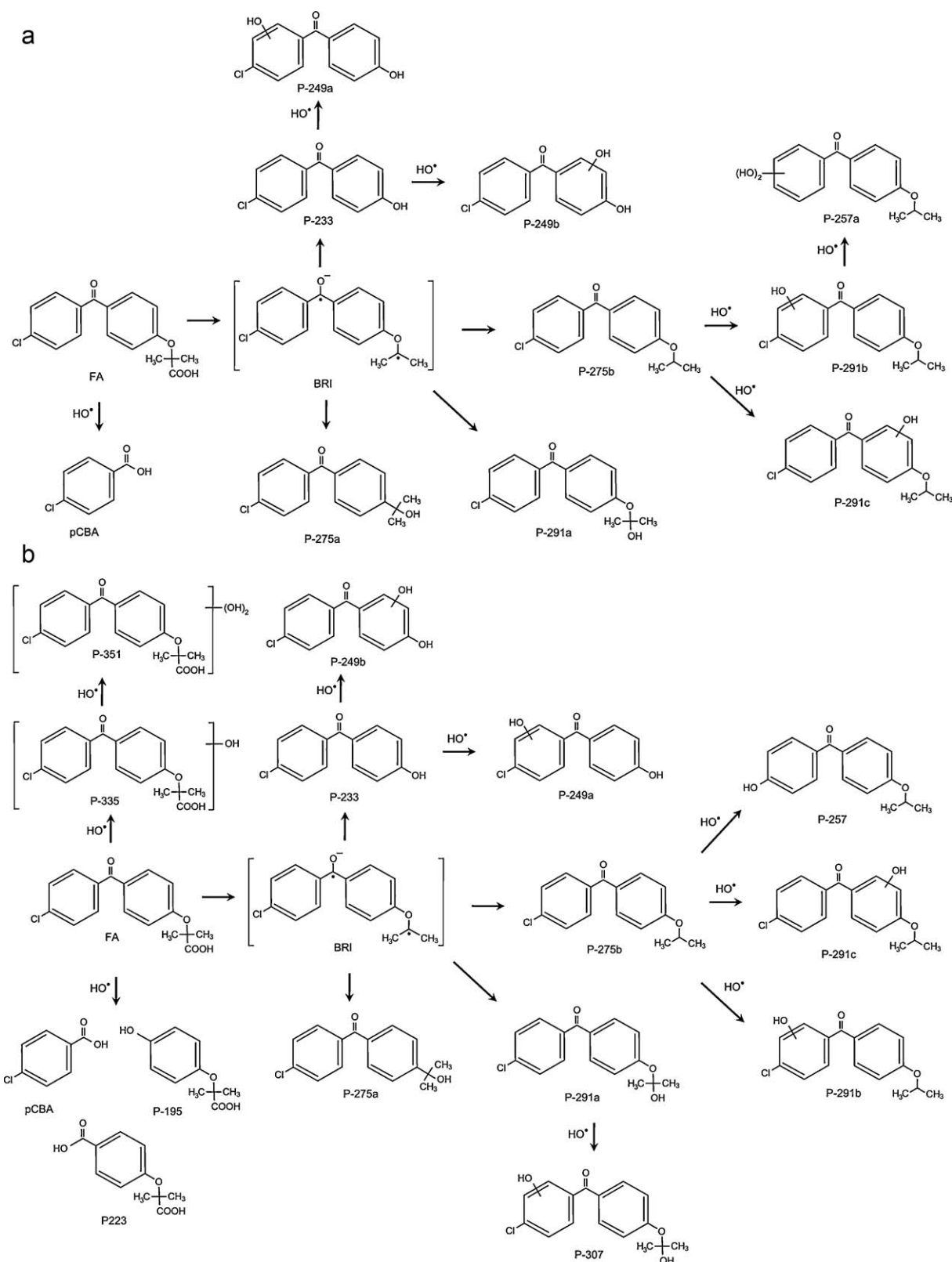


Fig. 6. Proposed reaction pathway for fenfibric acid under UV irradiation (a) and UV/H₂O₂ (b).

minor compound in all reaction mixtures, P-275b being the most abundant intermediate product in all cases. Fig. 7 shows the chromatographic areas corresponding to the compounds identified in Tables 1 and 2 by lumping certain minor products into a pseudo-component A. The data show that the toxicity of irradiated samples

and the recovery of toxicity at higher reaction times in the case of UV/H₂O₂ runs cannot be attributed to the formation or accumulation of a single compound, but are most probably the result of the production of several compounds with a similar chemical structure and toxicity. Is it noteworthy that most intermediates from

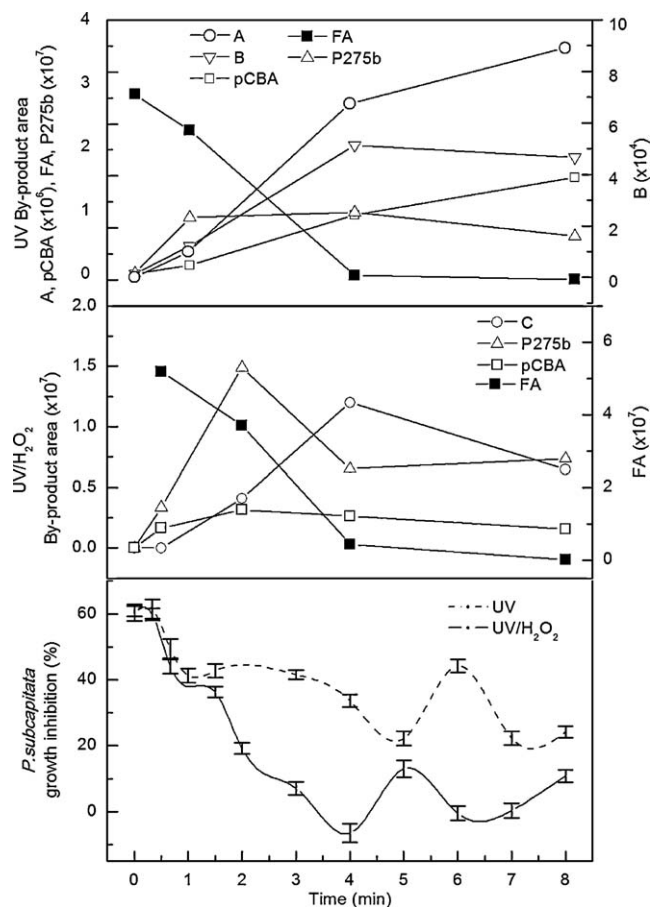


Fig. 7. Growth inhibition of *Pseudokirchneriella subcapitata* and chromatographic area of transformation products (A = P-291a + P-291b + P-291c, B = P-233 + P-249a + P-249b, C = P-307 + P-291a + P-291b + P-291c).

both UV and UV/H₂O₂ processes retained the chlorine atom and that the reduction of dissolved organic carbon was closely related to the extent of dechlorination. The higher toxicity of the UV irradiated mixtures was most probably the consequence of the presence of a higher concentration of chlorinated aromatics. The increase of toxicity observed in UV/H₂O₂ runs at high irradiation times was probably the consequence of the formation of ring-opening products, a kind of compound previously associated with high toxicity in partially oxidized mixtures [10].

4. Conclusions

The degradation of an aqueous solution of fenofibric acid using UV photolysis and UV/H₂O₂ led to the complete depletion of fenofibric acid for volume-based UV doses typically below 1 J cm⁻³. Quantum yields for fenofibric acid ranged from 0.039 ± 0.003 mol E⁻¹ (15 °C) to 0.088 ± 0.002 mol E⁻¹ (35 °C) with a photolytic activation energy of 21.5 ± 8.6 kJ mol⁻¹. The radical exposure per fluence ratio, R_{OH,UV}, was measured using pCBA as probe compound and reached a plateau of about 6 × 10⁻¹³ M cm² L mW⁻¹ at about 50 mg/L H₂O₂, before declining thereafter due to the hydroxyl radical scavenger role played by H₂O₂ at high concentration. The presence of fenofibric acid, a compound with intense UV absorption, decreased R_{OH,UV} considerably. Using competitive kinetics with atrazine, we obtained a second order rate constant of (5.56 ± 0.22) × 10⁹ M⁻¹ s⁻¹ for the reaction of fenofibric acid with hydroxyl radicals.

UV photolysis led to a low extent of dechlorination and mineralization reactions, typically below 10%. The maximum TOC removal

observed for UV/H₂O₂ was slightly over 50% after 4 min of reaction with most of the organic carbon being removed during the first minute. The absence of complete mineralization resulted in the accumulation of oxidation by-products identified using LC-ESI-QTOF-MS. Exact mass measurements allowed reaction pathways to be proposed for UV and UV/H₂O₂ that start with the decarboxylation of fenofibric acid before yielding 4-chloro-4'-(1-hydroxy-1-methylethyl)benzophenone and other minor products, predominantly chlorinated. We were also able to detect several intermediates from the reactions of primary products with hydroxyl radicals which, in the case of UV photolysis, were produced by the 185 nm ozone-forming emission of low-pressure mercury lamp. Some additional minor products were detected in ESI negative mode and corresponded to the scission of the carbonyl carbon to the aromatic carbon bond, the most abundant of which was pCBA.

We determined that the toxicity of UV irradiated samples for the 72 h growth of *P. subcapitata* was high even after the total depletion of fenofibric acid. This was attributed to the chlorinated aromatic products that dominated reaction mixtures at intermediate reaction times. There were low values for the toxicity of UV/H₂O₂ treated samples in which fenofibric acid was completely depleted. However, a degree of toxicity reappeared in highly irradiated mixtures, probably as a consequence of chlorinated reaction products.

Acknowledgements

This work has been financed by Spain's Ministry of Education (CSD2006-00044 and CTM2005-03080/TECNO) and the Dirección General de Universidades e Investigación de la Comunidad de Madrid, Research network 0505/AMB-0395. One of the authors, J.S., thanks the Spanish Ministry of Education for the award of an FPU grant.

References

- [1] R. Rosal, A. Rodríguez, J.A. Perdígón-Melón, A. Petre, E. García-Calvo, M.J. Gómez, A. Agüera, A.R. Fernández-Alba, Occurrence of emerging pollutants in urban wastewater and their removal through biological treatment followed by ozonation, *Water Res.* 44 (2010) 578–588.
- [2] M. Stumpf, T.A. Ternes, R.D. Wilken, S.V. Rodrigues, W. Baumann, Polar drug residues in sewage and natural waters in the state of Rio de Janeiro, Brazil, *Sci. Total Environ.* 225 (1999) 135–141.
- [3] T.A. Ternes, J. Stüber, N. Herrmann, D. McDowell, A. Ried, M. Kampmann, B. Teiser, Ozonation: a tool for removal of pharmaceuticals, contrast media and musk fragrances from wastewater? *Water Res.* 37 (2003) 1976–1982.
- [4] J.L. Acero, F.J. Benitez, A.I. Leal, F.J. Real, F. Teva, Membrane filtration technologies applied to municipal secondary effluents for potential reuse, *J. Hazard. Mater.* 177 (2010) 390–398.
- [5] R. Rosal, I. Rodea-Palomares, K. Boltes, F. Fernández-Piñas, F. Leganés, S. Gonzalo, A. Petre, Ecotoxicity assessment of lipid regulators in water and biologically treated wastewater using three aquatic organisms, *Environ. Sci. Pollut. Res.* 17 (2010) 135–144.
- [6] I. Rodea-Palomares, A. Petre, K. Boltes, F. Leganés, J.A. Perdígón-Melón, R. Rosal, F. Fernández-Piñas, Application of the combination index (CI)-isobologram equation to study the toxicological interactions of lipid regulators in two aquatic bioluminescent organisms, *Water Res.* 44 (2010) 427–438.
- [7] R. Rosal, I. Rodea-Palomares, K. Boltes, F. Fernández-Piñas, F. Leganés, A. Petre, Ecotoxicological assessment of surfactants in the aquatic environment: combined toxicity of docusate sodium with chlorinated pollutants, *Chemosphere* 81 (2) (2010) 288–293.
- [8] M.I. Litter, Introduction to photochemical advanced oxidation processes for water treatment, in: P. Boule, D.W. Bahnemann, P.K.J. Robertson (Eds.), *The Handbook of Environmental Chemistry*, Vol. 2, Part M, Environmental Photochemistry Part II, Springer-Verlag, Berlin Heidelberg, 2005, pp. 325–366.
- [9] B. Legube, Formation of ozonation by-products, in: A. Nikolay (Ed.), *The Handbook of Environmental Chemistry*, Vol. 5, Part G, Haloforms and Related Compounds in Drinking Water, Springer, Berlin, 2003, pp. 95–116.
- [10] R. Rosal, M.S. Gonzalo, K. Boltes, P. Letón, J.J. Vaquero, E. García-Calvo, Identification of intermediates and ecotoxicity assessment of the oxidation products generated during the ozonation of clofibric acid, *J. Hazard. Mater.* 172 (2009) 1061–1068.

- [11] J.J. López, M. Sánchez-Polo, C.V. Gómez-Pacheco, J. Rivera-Utrilla, Photodegradation of tetracyclines in aqueous solution by using UV and UV/H₂O₂ oxidation processes, *J. Chem. Technol. Biotechnol.* 85 (2010) 1325–1333.
- [12] G. Eisenberg, Colorimetric determination of hydrogen peroxide, *Ind. Eng. Chem. Anal. Ed.* 15 (1943) 327–328.
- [13] A.N. Baga, G.R.A. Johnson, N.B. Nazhat, R.A. Saadalla-Nazhat, A simple spectrophotometric determination of hydrogen peroxide at low concentrations in aqueous solution, *Anal. Chim. Acta* 204 (1988) 349–353.
- [14] I. Nicole, J. de Laat, M. Dore, J.P. Duguet, C. Bonnel, Use of UV radiation in water treatment: measurement of photonic flux by hydrogen peroxide actinometry, *Water Res.* 24 (1990) 157–168.
- [15] F.J. Beltrán, M. González, F.J. Rivas, J. Jaramillo, Application of photochemical reactor models to UV irradiation of trichloroethylene in water, *Chemosphere* 31 (1995) 2873–2885.
- [16] J.R. Bolton, M.I. Stefan, Fundamental photochemical approach to the concepts of fluence (UV dose) and electrical energy efficiency in photochemical degradation reactions, *Res. Chem. Intermediat.* 28 (2002) 857–870.
- [17] F.J. Benítez, J.L. Acero, F.J. Real, C. Maya, Modeling of photooxidation of acetamide herbicides in natural waters by UV radiation and the combinations UV/H₂O₂ and UV/O₃, *J. Chem. Technol. Biotechnol.* 79 (2004) 987–997.
- [18] F.J. Beltrán, G. Ovejero, B. Acedo, Oxidation of atrazine in water by ultraviolet radiation combined with hydrogen peroxide, *Water Res.* 27 (1993) 1013–1021.
- [19] M.A. Miranda, F. Bosca, F. Vargas, N. Canudas, Unusual (1, 2) Wittig rearrangement of a carbanion generated in neutral aqueous-medium by photodecarboxylation of a phenoxyacetic acid analogue, *J. Photochem. Photobiol. A: Chem.* 78 (1994) 149–151.
- [20] E.J. Rosenfeldt, K.G. Linden, The R_{OH,UV} concept to characterize and model UV/H₂O₂ processes in natural waters, in: *IUVA 2005: Third International Congress on Ultraviolet Technologies*, Whistler, British Columbia, May 24–27, 2005.
- [21] E.J. Rosenfeldt, K.G. Linden, S. Canonica, U. von Gunten, Comparison of the efficiency of OH radical formation during ozonation and the advanced oxidation processes O₃/H₂O₂ and UV/H₂O₂, *Water Res.* 40 (2006) 3695–3704.
- [22] B. Balci, N. Oturan, R. Cherrier, M.A. Oturan, Degradation of atrazine in aqueous medium by electrocatalytically generated hydroxyl radicals. A kinetic and mechanistic study, *Water Res.* 43 (2009) 1924–1934.
- [23] R. Rosal, M.S. Gonzalo, A. Rodríguez, E. García-Calvo, Catalytic ozonation of fenofibric acid over alumina-supported manganese oxide, *J. Hazard. Mater.* 183 (2010) 271–278.
- [24] M. Cermola, M. DellaGreca, M.R. Iesce, L. Previtera, M. Rubino, F. Temussi, M. Brigante, Phototransformation of fibrates drugs in aqueous media, *Environ. Chem. Lett.* 3 (2005) 43–47.
- [25] G. Cosa, Photodegradation and photosensitization in pharmaceutical products: assessing drug phototoxicity, *Pure Appl. Chem.* 76 (2004) 263–275.
- [26] F. Bosca, M.A. Miranda, A laser photolysis study on fenofibric acid, *Photochem. Photobiol.* 70 (1999) 853–857.
- [27] J. Thomson, F. Roddick, M. Drikas, Natural organic matter removal by enhanced photo-oxidation using low-pressure mercury vapour lamps, *Water Sci. Technol.* 2 (2002) 435–443.